nature materials

ARTICLES

PUBLISHED ONLINE: 19 JUNE 2011 | DOI: 10.1038/NMAT3051

Giant Rashba-type spin splitting in bulk BiTeI

K. Ishizaka[1]*, M. S. Bahramy[2], H. Murakawa[3], M. Sakano[1], T. Shimojima[1], T. Sonobe[1], K. Koizumi[4], S. Shin[4,5], H. Miyahara[6], A. Kimura[6], K. Miyamoto[7], T. Okuda[7], H. Namatame[7], M. Taniguchi[6,7], R. Arita[1,2], N. Nagaosa[1,2], K. Kobayashi[8], Y. Murakami[8], R. Kumai[8,9], Y. Kaneko[3], Y. Onose[1,3] and Y. Tokura[1,2,3]

There has been increasing interest in phenomena emerging from relativistic electrons in a solid, which have a potential impact on spintronics and magnetoelectrics. One example is the Rashba effect, which lifts the electron-spin degeneracy as a consequence of spin–orbit interaction under broken inversion symmetry. A high-energy-scale Rashba spin splitting is highly desirable for enhancing the coupling between electron spins and electricity relevant for spintronic functions. Here we describe the finding of a huge spin–orbit interaction effect in a polar semiconductor composed of heavy elements, BiTeI, where the bulk carriers are ruled by large Rashba-like spin splitting. The band splitting and its spin polarization obtained by spin- and angle-resolved photoemission spectroscopy are well in accord with relativistic first-principles calculations, confirming that the spin splitting is indeed derived from bulk atomic configurations. Together with the feasibility of carrier-doping control, the giant-Rashba semiconductor BiTeI possesses excellent potential for application to various spin-dependent electronic functions.

The Rashba effect was originally discussed in seminal studies describing the spin–orbit interaction (SOI)-induced **k**-linear (**k**: electron momentum) band splitting in non-centrosymmetric wurtzite semiconductors[1,2], as represented by the cases of CdS and CdSe. Later, the Bychkov–Rashba model[3] was proposed to simply describe the motion of an electron in a two-dimensional electron gas (2DEG) system with a potential gradient (that is, electric field $\mathbf{E}_z$) along the normal to the 2DEG plane, thus triggering the spintronic investigation involving interfaces and surfaces. An electron with **k** and spin $\boldsymbol{\sigma}$ in such a 2DEG experiences an effective magnetic field induced by $\mathbf{E}_z$, as represented by the **k**-linear Rashba Hamiltonian, $H_R = \lambda\, \boldsymbol{\sigma} \cdot (\mathbf{E}_z \times \mathbf{k})$, with coupling constant λ. Owing to this SOI effect, the spin-degenerate parabolic bands split into dispersions with oppositely spin-polarized states, whose energy values are denoted by $E^{\pm}(\mathbf{k}) = (\hbar^2\mathbf{k}^2/2m^*) \pm \alpha_R|\mathbf{k}|$, where m^* represents the effective mass of electrons. Here, α_R ($\propto \lambda E_z$) is called a Rashba parameter and represents the strength of the Rashba effect. This effect has been demonstrated in semiconductor heterostructure[4], and directly confirmed in the surface Shockley states of heavy metals by spin-, angular-resolved photoemission spectroscopy[5,6]. Recently, the discovery of a giant Rashba-type splitting realized at noble-metal-based surface alloys[7] has been attracting much interest, where heavy elements with a strong atomic SOI are incorporated into the surface. In addition to the investigation of the enhanced Rashba splitting, efforts to transfer it from metal to semiconductor substrates are also being made[8], to remove the presence of spin-degenerate carriers that hinder the spintronic functions. The realization of such electron systems with high-energy-scale Rashba splitting will provide opportunities for practical spintronic applications[9], as well as hosting non-trivial phenomena such as intrinsic spin Hall effect[10] and non-centrosymmetric exotic superconductivity[11].

Here we show that a layered polar semiconductor BiTeI forms a huge spin-split band derived from its bulk polar atomic configuration. The crystal structure of trigonal BiTeI ($P3m1$) and the corresponding first Brillouin zone are shown in Fig. 1a,b, respectively. The structure is characterized by a sequence of triangular network layers composed of Bi, Te and I. Previous structural analysis study[12] indicates that the structure of BiTeI can be described in terms of a semi-ionic model, where the covalent coupling of Bi and Te atoms forms positively charged $(BiTe)^+$ layers, whereas Bi–I contacts are considered to be ionic. Thus, the crystal structure possesses a semi-ionic polar axis along the stacking direction, while maintaining three-fold in-plane rotational symmetry. Owing to this rather simple crystal structure compared with some previously studied non-centrosymmetric compounds[13,14], the band structure and the SOI effect are also simple. The in-plane electric resistivity measured using a single-crystalline BiTeI sample as shown in Fig. 1c indicates a metallic behaviour down to 2 K. The Hall coefficient is temperature independent, and the estimated electron concentration is $n_H = 4.5 \times 10^{19}$ cm^{-3}. Thus this compound behaves as a degenerate n-type semiconductor because of possible non-stoichiometry[15].

The result of a relativistic first-principles band calculation is shown in Fig. 1d. The bands above the Fermi level (E_F) are mostly derived from the three Bi $6p$ levels, whereas those below E_F are dominantly from six bands of Te and I $5p$ levels. As compared with the result without spin–orbit coupling, the overall band structures are strongly modified by splitting of bands, reflecting the spin-splitting effect from broken inversion symmetry. Along the Γ–A

[1]Department of Applied Physics, University of Tokyo, Tokyo 113-8656, Japan, [2]Correlated Electron Research Group (CERG), RIKEN-ASI, Wako 351-0918, Japan, [3]Multiferroics Project, ERATO, JST, Tokyo 113-8656, Japan, [4]Institute for Solid State Physics, University of Tokyo, Kashiwa, 277-8581, Japan, [5]CREST, JST, Tokyo 102-0075, Japan, [6]Graduate School of Science, Hiroshima University, Higashi-Hiroshima 739-8526, Japan, [7]Hiroshima Synchrotron Radiation Center, Hiroshima University, Higashi-Hiroshima 739-0046, Japan, [8]Condensed Matter Research Center, Institute of Materials Structure Science, KEK, Tsukuba, 305-0801, Japan, [9]National Institute of Advanced Industrial Science and Technology (AIST), Tsukuba 305-8562, Japan.
*e-mail: ishizaka@ap.t.u-tokyo.ac.jp.

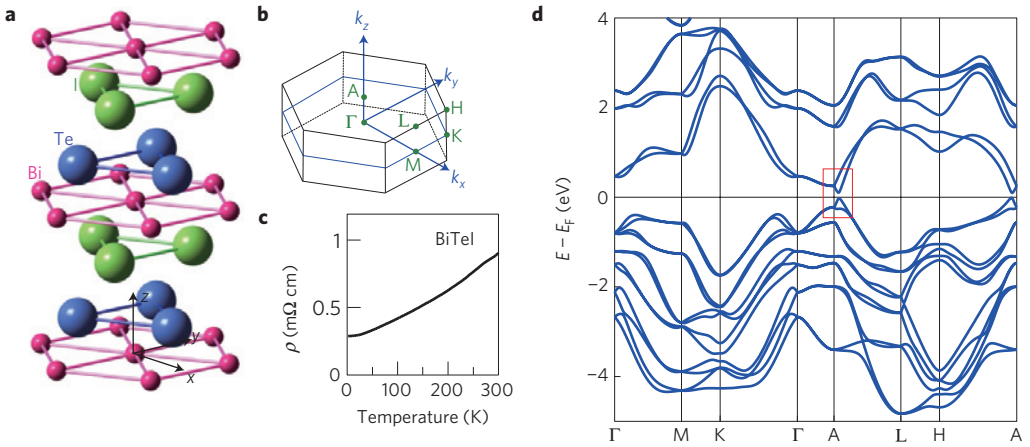

Figure 1 | Basic properties of BiTeI. a, Crystal structure. **b**, Brillouin zone. **c**, Temperature-dependent electrical resistivity. **d**, Energy-band dispersions obtained by relativistic first-principles band calculation.

($\mathbf{k}_\parallel = (k_x, k_y) = 0$) direction, the spin degeneracy is maintained, and the moderate k_z dispersion can be recognized, with the conduction-band minimum (CBM) and the valence-band maximum (VBM) appearing at $k_z = \pi/c$. For $k_\parallel \neq 0$, the band dispersions are subject to large splitting with typical energies of 0.1–0.2 eV. Because of these splittings, the CBM is located slightly off the A point in the $k_z = \pi/c$ plane, thus forming a Rashba-like dispersion (see inside the red rectangle in Fig. 1d). Assuming that the doping simply induces a rigid band shift, the chemical potential corresponding to the bulk electron density $n = 4.5 \times 10^{19}$ cm^{-3} is calculated to be 0.142 eV above the CBM. It is worth noting that this chemical potential is very close to the band crossing point at the A point ($k_\parallel = 0$).

Figure 2a–c shows the result of angle-resolved photoemission spectroscopy (ARPES) using the photon energy of $h\nu = 21.2$ eV. The first Brillouin zone with the mapping of ARPES intensity at E_F is shown in Fig. 2a, whereas the ARPES image along the k_x direction (shown with the red line in Fig. 2a) is plotted in Fig. 2c. It clearly shows the Rashba-like split bands with CBM of $E_{CBM} = 0.29$ eV at the momentum offsets of $\pm k_0$ with $k_0 = 0.052$ Å^{-1}. At the binding energy (E_B) of ~0.6 eV, the valence-band top with similar splitting can also be discerned. These band features correspond well to the $k_z = \pi/c$ part of the band calculation in Fig. 1d; nevertheless, the CBM energy of 0.29 eV is considerably deeper than expected by calculation (0.142 eV at $k_z = \pi/c$). This probably indicates that the observed dispersion corresponds to the bulk CBM being shifted downward because of the near-surface band-bending effect, as will be discussed later. To estimate the bandgap between the CBM and VBM, the angle-integrated PES recorded at around $k_\parallel = 0$ is plotted in Fig. 2b. The CBM and VBM positions are located at the binding energies of ~0.29 and ~0.67 eV, respectively, thus providing the gap of ~0.38 eV.

To grasp the overall character of split conduction-band dispersions, the constant-E_B contours are shown in Fig. 2c (right panels) as a function of k_x and k_y, for respective E_B. At $E_B = 0$ it corresponds to the intensity map at E_F, where the two Fermi surfaces (outer and inner) characteristic of the Rashba-type splitting are apparent. Their shapes are nearly circular with slight triangular contrast of intensity, reflecting the three-fold in-plane rotational symmetry. On increasing E_B, both the outer and inner band contours get smaller. At $E_B \sim 0.18$ eV, the inner contour becomes very small as it makes a crossing point at $k_x = k_y = 0$. On increasing E_B, the outer one becomes smaller while the inner gets slightly larger, and they almost merge with each other and form a broad triangular-ring valley ($E_B \sim 0.27$–0.36 eV), which corresponds to the CBM. Passing through the bandgap, the top of the VBM gradually becomes visible ($E_B \sim 0.55$ eV), showing

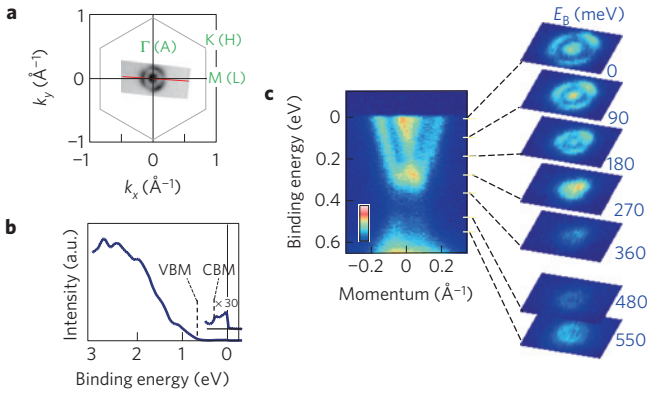

Figure 2 | Rashba-split conduction bands observed by ARPES ($h\nu = 21.2$ eV). a, Fermi-surface mapping overlaid on the two-dimensional Brillouin zone of BiTeI. **b**, Angle-integrated PES around the $k_\parallel = 0$ region. The near-E_F part is magnified (×30) to show the conduction-band structure. **c**, The ARPES image of the Rashba-split conduction bands. The right panels show the band contour images as functions of k_x and k_y at certain binding energies.

up as a small ring-like feature with the radius of ~ 0.05 Å^{-1}. Eventually, the observed CBM and VBM indicate similar sizes of splitting with ~k_0, showing a very good accordance with the band calculation at $k_z \sim \pi/c$.

To quantitatively discuss the splitting, a close-up of the conduction band and the corresponding Fermi surface observed by ARPES are shown in Fig. 3a,b, respectively. The plotted markers are the peak positions of energy- and/or momentum-distribution curves. The red (blue) markers in Fig. 3a represent the $\sigma_\perp > 0$ 'spin-up' ($\sigma_\perp < 0$ 'spin-down') component as observed in spin-resolved ARPES (SRARPES) data shown in Fig. 3c,d. Here, $\sigma_\perp$ denotes the spin component along the direction perpendicular to the surface normal and to the photoemission vector. Figure 3c shows the spin-polarization image, obtained from the subtraction of spin-up and spin-down intensities as shown in Fig. 3d. It is apparent from these data that the left (right) band dispersion with its bottom at $k = -k_0$ ($k = +k_0$) is dominated by spin-up (spin-down) intensity. This is very similar to the spin splitting observed in surface states of noble metals and their surface alloys[5,7,16]. To confirm this behaviour theoretically, the spin-dependent band dispersions and Fermi surface are calculated by the relativistic first-principles method (Fig. 3e,f). A close-up of the calculated conduction-band bottom at $k_z = \pi/c$ is shown in Fig. 3e. Here, the binding energy

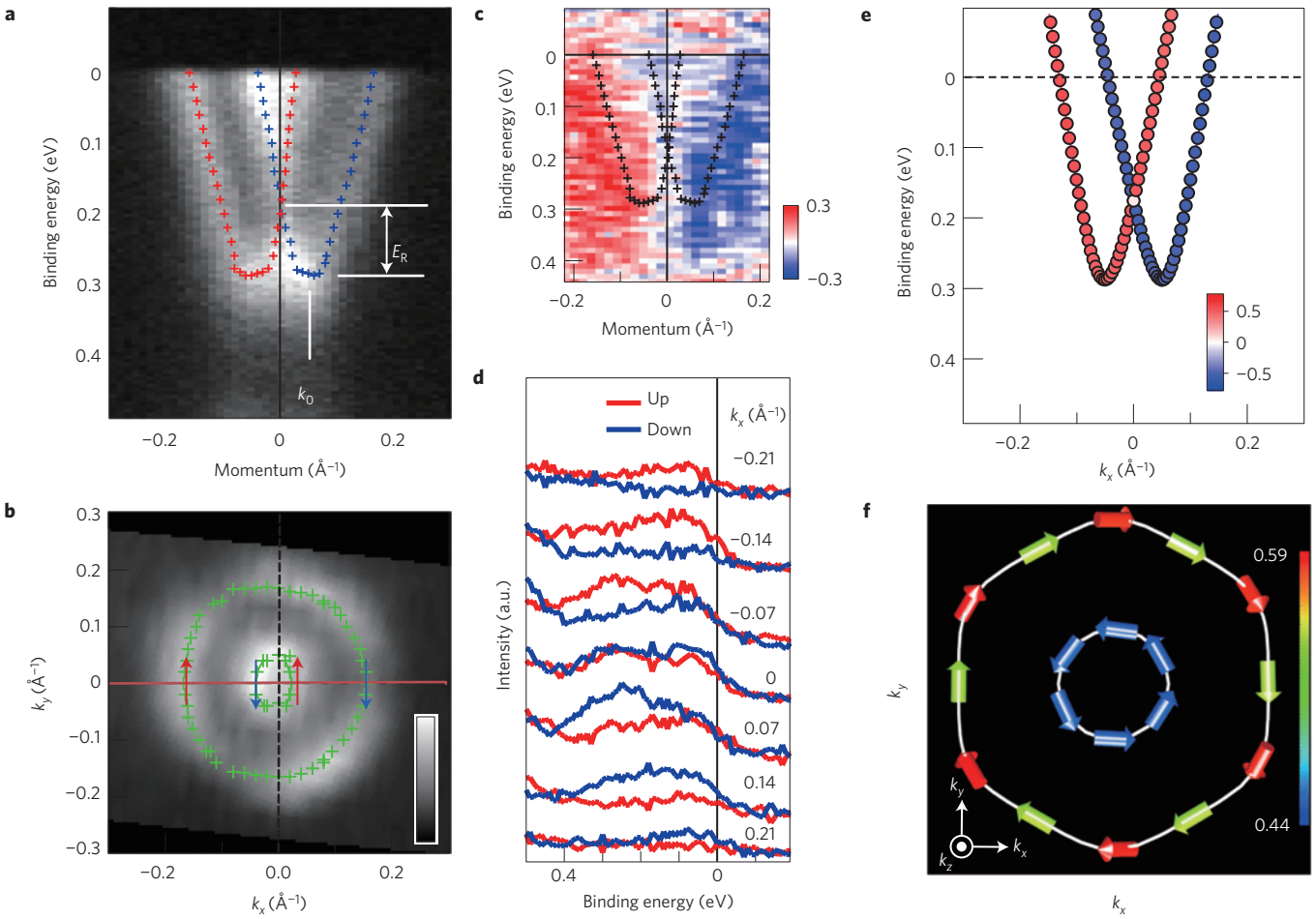

Figure 3 | Spin polarization of Rashba-split bands. a, Markers tracking the band dispersions overlaid on the ARPES intensity image. The markers show the peak positions of the EDCs and MDCs. Red (blue) markers represent the $\sigma_\perp > 0$ 'spin-up' ($\sigma_\perp < 0$ 'spin-down') components, as confirmed by SRARPES shown in **c**,**d**. **b**, The Fermi-surface map. Green markers show the peak positions of MDCs at E_F. The red line represents the momentum cut of the SRARPES images in **c**,**d**. **c**, The spin-polarization image obtained by SRARPES. **d**, The EDCs of SRARPES measured along k_x. The red (blue) curves show the spin-up (spin-down) components. **e**, Calculated spin polarization on conduction-band dispersions along A–L ($k_y = 0, k_z = \pi/c$). Only the $\sigma_\perp$-component is shown by the colour scale for comparison with the experiment. **f**, Calculated spin polarization overlaid on the Fermi surface at $k_z = \pi/c$. The arrows show the orientation of spin whereas their colour indicates the degree of polarization.

(left axis) is rigidly shifted to match the CBM energy with the experiment, to account for the band-bending effect. The colour shows the polarization of the spin component $\sigma_\perp$ in units of $\hbar/2$ for respective bands and k points. The spin splitting (for example k_0) as well as the detailed character of band dispersions are in excellent accordance with the experimental result in Fig. 3a. This thus strongly suggests that this Rashba-like splitting is derived from the bulk atomic configuration, not from surface states or the near-surface band-bending effect. It is also essentially different from the very recently observed Rashba-like spin polarization in the ARPES spectrum of the bulk continuum states keeping the spin degeneracy, arising from the reflection of the relativistic Bloch waves from the surface barrier, which leads to a beating of the spin density[17].

The characteristic parameters quantifying the strength of the Rashba splitting in addition to the momentum offset k_0 are the Rashba energy E_R and the coupling constant α_R (Rashba parameter). They are related by $E_R = \hbar^2 k_0^2/2m^*$ and $k_0 = m^*\alpha_R/\hbar^2$ in a 2DEG model. Here we evaluate the spin splitting of the conduction band in BiTeI by analogy. Our present result along the k_x (A–L) direction shows that $k_0 \sim 0.052$ Å^{-1}, and $E_R \sim 0.1$ eV ($= E_{cross} - E_{CBM}$) with $E_{CBM} = 0.29$ eV, $E_{cross} = 0.19$ eV. From E_R and k_0, we can evaluate the Rashba parameter as $\alpha_R = 3.85$ eVÅ. This value, though including some extent of uncertainty due to the band dispersion's deviation from the 2DEG assumption $E = \hbar^2 k^2/2m^*$, is one of the largest among the Rashba splittings observed in various systems (Table 1).

Through the recent studies on surface states of metals[5,16] and a number of surface alloys, it has been found that the in-plane in addition to the out-of-plane component of the potential gradient plays a crucial role in enhancing the level of spin splitting. For example, in Bi/Ag(111) (ref. 7) or Bi/Si(111) (ref. 8), the evaporated Bi atoms are incorporated into the substrate, and form a reconstructed surface alloy state with $\sqrt{3} \times \sqrt{3}$ structure. The further reduced symmetry induces the in-plane gradient, deforming the Fermi surface from an ideally circular to a hexagonal shape. At the same time, it also rotates the spin orientation away from the genuine Rashba orientation (that is, perpendicular to the surface normal and **k**), and significantly enhances the splitting[7]. In contrast, it is interesting to note that the ultrathin films of Bi (and Pb) show no or, at most, a very weak splitting among their quantum-well subband states, even though the surface states in the same Bi film are dominated by substantial splitting[18,19]. The only exception until now is the unoccupied subband state of one monolayer of Bi on Cu(111) (ref. 20), which shows a giant splitting. This has been elucidated by the speculation that the wavefunction of the quantum-well state is located quite far from the surface or interface and does not experience a large enough potential gradient. Other possibilities are also raised that

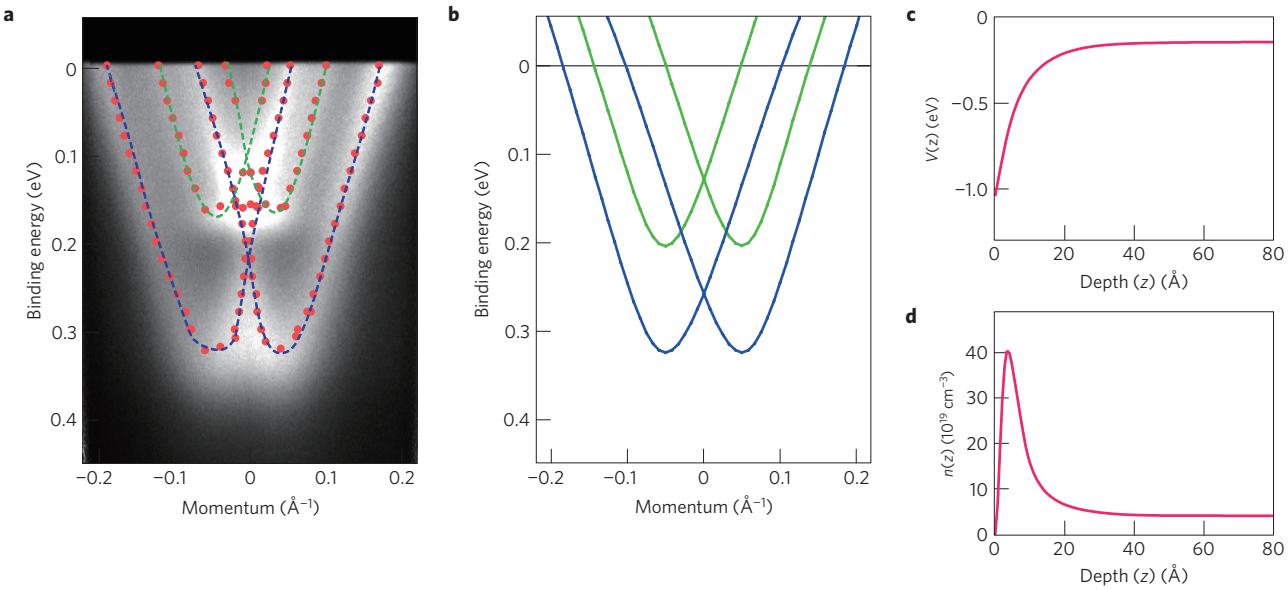

Figure 4 | Subband structure of Rashba-split conduction band quantized in the band-bending accumulation layer. a, ARPES image along k_x obtained by an $h\nu = 6.994$ eV laser light source. The red markers show the peak positions of the EDC and MDC. The blue (green) curve is a guide for the eyes to trace the dispersions of the $n = 1$ ($n = 2$) subband. **b**, Calculated subband structures taking into account the quantization of the conduction band in the two-dimensional surface accumulation layer. **c**, The calculated potential energy as a function of the depth from the surface (z). **d**, The calculated electron density as a function of z.

Table 1 | Selected materials and parameters characterizing spin band splitting: the momentum offset k_0 (Å^{-1}), Rashba energy E_R (meV) and Rashba parameter α_R (eV Å).

Sample	k_0	E_R	α_R	Reference
Surface state				
Au(111)	0.012	2.1	0.33	5
Bi(111)	0.05	14	0.55	16
1/3 ML Bi on Ag surface alloy	0.13	200	3.05	7
Interface				
InGaAs/InAlAs	0.028	<1	0.07	4
QW state				
Pb thin film (6–22 ML)	0.035	$\lesssim$10	0.04	36
Bi thin film (7–40 BL)	-	-	-	18,37
1 ML Bi on Cu	N/A	N/A	2.5	20
Bulk				
BiTeI	0.052	100	3.8	This work

For the Bi thin-film system in refs 18,37, the splitting was observed only for the surface states, not for the QW subband states. ML, monolayer.

quantum-well states should show no Rashba splitting because of their standing-wave character, or that the competing effects at both surface and interface reduce the net spin–orbit splitting.

In the present case of BiTeI, the inner Fermi surface turns out to be well describable by a simple Rashba model linear in terms of k. On the other hand, the calculated outer Fermi surface at $k_z = \pi/c$ seems to deviate from a perfect circular shape, and instead shows a hexagonal shape. Such anisotropy is attributed to the higher-order splitting terms in $P3m1$ symmetry beyond the k-linear Rashba model, becoming discernible at this fairly large-k region[21–23]. In particular, the appearance of the out-of-plane spin component (σ_z) for the outer Fermi surface at certain k points (see Fig. 3f) is a characteristic feature of the trigonal (C_{3v}) symmetry of BiTeI. The respective effective Hamiltonian, as already established in the context of zinc-blende materials[22,23], is expected to be proportional to $(3k_x^2 - k_y^2)k_y\sigma_z$. The experimental Fermi surfaces show a more or less circular shape; nevertheless, the three-fold symmetry shows up as the weak triangular distortion and the intensity contrast. Detection of $\sigma_{\|}$ (the spin component along the photoemission vector) and σ_z, for example by multidetector SRARPES, remains to be further investigated to fully understand the microscopic picture of this giant spin splitting appearing in BiTeI.

The Rashba-split conduction bands with the bottom at around 0.3 eV, as we have discussed, are similarly observed with other photon energies (for example $h\nu = 40.8$ eV). This indicates that they are a fairly k_z-independent two-dimensional electronic structure, arising from the near-surface band-bending layer. Also considering that the observed CBM energy is rather deeper than expected from the bulk electron density, ARPES measurements should be looking at the 'bulk' conduction band shifted downward through the near-surface band-bending effect. This can be confirmed by the ARPES image along k_x obtained by using $h\nu = 6.994$ eV as shown in Fig. 4a. The red markers indicate the estimated peak positions of the momentum-distribution curve (MDC) and energy-distribution curve (EDC). Apparently, there are extra band structures compared with $h\nu = 21.2$ eV (Fig. 3a): another set of Rashba-split bands with lower binding energies. This is perhaps due to the deeper probing depth ($l \lesssim 80$ Å) and/or high momentum resolution of the $h\nu = 6.994$ eV ARPES as compared with the $h\nu = 21.2$ eV ARPES ($l \lesssim 4$ Å; ref. 24). The blue curves show the deeper bands with the bottoms at 0.33 eV, whereas the green curves trace the shallower bands with bottoms at 0.17 eV, as guides for the eyes. These dispersions can be understood as quantized subbands of the bulk conduction band, $n = 1$ and $n = 2$ respectively, due to the two-dimensional electronic confinement within the surface band-bending layer. Such subband structures are known to be observed in quantum-well systems, for example ultrathin-film metals[18,19] and semiconductor near-surface depletion layers[25]. Very recently, the downward shift of the conduction band and its confinement in the near-surface electron-accumulation layers, resulting in n-type subband formation, are also reported to be realized in some n-type semiconductors[26]. This resembles our case.

To simulate our present result, we adopted the Poisson–Schrödinger equation method as described in ref. 27. Here we

consider the potential energy $V(z)$ and electron density $n(z)$ as functions of the depth from the surface z (see Methods for details). From the Fermi surfaces in Fig. 3b showing the nearly circular shapes with Fermi momenta of $k_F^{\rm out} \sim 0.17\,\text{Å}^{-1}$ and $k_F^{\rm in} \sim 0.04\,\text{Å}^{-1}$, we can estimate the electron density at the topmost surface layer as $n_{\rm surface} = 4 \times 10^{20}\,\text{cm}^{-3}$. In contrast, $n(z \to \infty)$ can be assumed as the bulk electron density, $n_{\rm bulk} = n_{\rm H} = 4.5 \times 10^{19}\,\text{cm}^{-3}$. With these constraints, $V(z)$ and $n(z)$ shown in Fig. 4c,d are obtained, which most well reproduce the observed data as given in Fig. 4b. The dielectric constant used here is $\epsilon/\epsilon_0 \sim 5$. This result indicates that there exists a band-bending layer with a thickness of $d \sim 20$ Å, where the electron accumulation of $\sim 10 \times n_{\rm bulk}$ is attained. Owing to the fact that the CBM in the bulk is located at $k_z = \pi/c$, the low-energy quantum-well subbands are mostly characterized by the band dispersion near the A point. It thus brings the spin-split CBM almost rigidly from 0.142 eV below $E_{\rm F}$ in the bulk down to 0.3 eV below $E_{\rm F}$ at the surface, as observed by ARPES. Here we should stress that this giant Rashba-type splitting is not due to the quantum-well accumulation-layer formation; the potential gradient arising from the band bending can also further affect the splitting, but this is expected to be small compared with the energy scale of $E_{\rm R} \sim 0.1$ eV. As we have mentioned, the observed band dispersion and its splitting agree very well with the first-principles calculation, thus offering strong supporting evidence for its bulk nature. This giant bulk Rashba-split system will bring out a number of anomalous magnetotransport/optical effects[28,29] that involve all the spin-polarized carriers from the bulk. The control of the carrier density by doping will further make the series of Rashba-split insulator, p and n-type semiconductor, and metal samples available, which might also lead to the development of novel superconductors.

Methods

Sample preparation. Single crystals of BiTeI were grown by the Bridgman method. Pure powders of bismuth, tellurium and iodine with the ratio of 1:1:1 were mixed in a quartz ampoule with a conical tip, which was sealed in vacuum and then inserted into a vertical furnace. After melting the sealed sample above 600 °C, the ampoule was pulled with a speed of 2 mm h^{-1} toward the lower-temperature region to obtain the single crystals. With these procedures, however, some contamination (typically BiI_3) was also produced as an impurity phase. We found that the initial substitution of a tiny amount of Bi by Mn was effective for reducing the impurity phase and for improving the quality of the BiTeI single crystal. The resistivity and the Hall resistivity of this refined crystal is essentially the same as that of the crystal grown without Mn substitution, thus indicating that the Mn is not playing a substantial role as a dopant. The crystal structure of the obtained specimen was determined by X-ray diffraction measurement. For photoemission spectroscopy measurements, the samples were cleaved at 200 K *in situ* with a vacuum of 1×10^{-10} torr during the measurement. By low-energy electron diffraction measurements, the cleaved crystal (001) surfaces were confirmed to be free from any reconstruction, showing clear 1×1 diffraction patterns.

Angular-resolved photoemission spectroscopy (ARPES). ARPES measurement ($h\nu = 21.2$ eV) was made at the Institute of Solid State Physics, University of Tokyo, using a VUV5000 He-discharge lamp and an R4000 hemispherical electron analyser (VG-Scienta). The total energy resolution was set to 20 meV. ARPES measurement ($h\nu = 6.994$ eV) was also made at the Institute of Solid State Physics, University of Tokyo, using a vacuum-ultraviolet-laser light source and R4000 (VG-Scienta)[30]. The total energy resolution was set to 2.5 meV. The temperature of measurement was 6 K unless otherwise noted.

Spin- and angle-resolved photoemission (SRARPES). SRARPES measurement ($h\nu = 21.2$ eV) was made at the Hiroshima Synchrotron Radiation Center. The spectra were recorded at 130 K using unpolarized He 1α radiation with a compact Mott detector operating at 25 keV (ref. 31). The angular resolution was ±1° and the energy resolution was set to 200 meV. In our measurement geometry, we can obtain the in-plane spin polarization of the spin component perpendicular to the plane spanned by the two vectors directed along the light incidence and electron emission. We define the spin direction as 'up' and 'down' with respect to this plane. The spin polarization P is obtained from $P = (1/S_{\rm eff})(I_{\rm U} - I_{\rm D})/(I_{\rm U} + I_{\rm D})$, where $I_{\rm U}$ and $I_{\rm D}$ are the measured intensities of the respective detectors, and $S_{\rm eff} = 0.128$ is the Sherman function. The spin-up and spin-down spectra are obtained by $I^{\uparrow,\downarrow} = (I_{\rm U} + I_{\rm D})(1 \pm P)/2$.

Electronic-structure calculation. Calculations were carried out within the context of density functional theory using the full-potential augmented plane-wave plus local orbital method, as implemented in the WIEN2K code[32]. Relativistic effects, including spin–orbit coupling, were fully taken into account. The exchange–correlation part of the potential was treated using the exchange–correlation functional of Perdew–Burke–Ernzerhof[33]. For all the atoms, the muffin-tin radius $R_{\rm MT}$ was set to 2.5 Bohr and the maximum modulus for the reciprocal vectors $K_{\rm max}$ was chosen such that $R_{\rm MT}K_{\rm max} = 7$. Taking the experimental lattice parameters $a = 4.340$ Å and $c = 6.854$ Å, the ionic positions were fully optimized until the magnitude of the force on each ion became less than 0.1 mRy Bohr^{-1}. The corresponding Brillouin zone was sampled by a $20 \times 20 \times 20$ k mesh. For the surface band-bending calculations, we adopted the non-parabolic coupled Poisson–Schrödinger approach of ref. 27. In our approach, the non-parabolicity of the conduction bands as well as the anisotropy of the effective mass were treated by constructing an effective model Hamiltonian for describing the 12 valence and six conduction bands below and above the Fermi level, respectively, using the maximally localized Wannier functions[34,35]. The dielectric constant was fixed at 5. The Fermi level was set to 142 meV above the CBM, corresponding to the experimentally observed bulk carrier density of $4.5 \times 10^{19}\,\text{cm}^{-3}$.

Received 27 January 2011; accepted 19 May 2011; published online 19 June 2011

References

1. Rashba, E. I. Properties of semiconductors with an extremum loop. 1. Cyclotron and combinational resonance in a magnetic field perpendicular to the plane of the loop. *Sov. Phys. Solid State* **2,** 1109–1122 (1960).
2. Casella, R. C. Toroidal energy surfaces in crystals with wurtzite symmetry. *Phys. Rev. Lett.* **5,** 371–373 (1960).
3. Bychkov, Y. A. & Rashba, E. I. Properties of a 2D electron gas with lifted spectral degeneracy. *JETP Lett.* **39,** 78–81 (1984).
4. Nitta, J., Akazaki, T., Takayanagi, H. & Enoki, T. Gate control of spin–orbit interaction in an inverted $In_{0.53}Ga_{0.47}As/In_{0.52}Al_{0.48}As$ heterostructure. *Phys. Rev. Lett.* **78,** 1335–1338 (1997).
5. LaShell, S., McDougall, B. A. & Jensen, E. Spin splitting of Au(111) surface state band observed with angle resolved photoelectron spectroscopy. *Phys. Rev. Lett.* **77,** 3419–3422 (1996).
6. Hoesch, M. *et al.* Spin structure of the Shockley surface state on Au(111). *Phys. Rev. B* **69,** 241401 (2004).
7. Ast, C. R. *et al.* Giant spin splitting through surface alloying. *Phys. Rev. Lett.* **98,** 186807 (2007).
8. Gierz, I. *et al.* Silicon surface with giant spin splitting. *Phys. Rev. Lett.* **103,** 046803 (2009).
9. Datta, S. & Das, B. Electronic analog of the electro-optic modulator. *Appl. Phys. Lett.* **56,** 665–667 (1990).
10. Sinova, J. *et al.* Universal intrinsic spin Hall effect. *Phys. Rev. Lett.* **92,** 126603 (2004).
11. Bauer, E. *et al.* Heavy fermion superconductivity and magnetic order in noncentrosymmetric $CePt_3Si$. *Phys. Rev. Lett.* **92,** 027003 (2004).
12. Shevelkov, A. V., Dikarev, E. V., Shpanchenko, R. V. & Popovkin, B. A. Crystal structures of bismuth tellurohalides BiTeX (X = Cl, Br, I) from X-ray powder diffraction data. *J. Solid State Chem.* **114,** 379–384 (1995).
13. Hashimoto, S. *et al.* The de Haas-van Alphen effect and the Fermi surface in $CePt_3Si$ and $LaPt_3Si$. *J. Phys. Condens. Matter* **16,** L287–L296 (2004).
14. Lee, K. W. & Pickett, W. E. Crystal symmetry, electron–phonon coupling, and superconducting tendencies in Li_2Pd_3B and Li_2Pt_3B. *Phys. Rev. B* **72,** 174505 (2005).
15. Tomokiyo, A., Okada, T. & Kawano, S. Phase diagram of system (Bi_2Te_3)–(BiI_3) and crystal structure of BiTeI. *Jpn. J. Appl. Phys.* **16,** 291–298 (1977).
16. Koroteev, Y. M. *et al.* Strong spin–orbit splitting on Bi surfaces. *Phys. Rev. Lett.* **93,** 046403 (2004).
17. Kimura, A. *et al.* Strong Rashba-type spin polarization of the photocurrent from bulk continuum states: Experiment and theory for Bi(111). *Phys. Rev. Lett.* **105,** 076804 (2010).
18. Hirahara, T. *et al.* Role of spin–orbit coupling and hybridization effects in the electronic structure of ultrathin Bi films. *Phys. Rev. Lett.* **97,** 146803 (2006).
19. Hirahara, T. *et al.* Direct observation of spin splitting in bismuth surface states. *Phys. Rev. B* **76,** 153305 (2007).
20. Mathias, S. *et al.* Quantum-well induced giant spin–orbit splitting. *Phys. Rev. Lett.* **104,** 066802 (2010).
21. Lo, I. *et al.* Anomalous k-dependent spin splitting in wurtzite $Al_xGa_{1-x}N/GaN$ heterostructures. *Phys. Rev. B* **75,** 245307 (2007).
22. Wang, W. T. *et al.* Dresselhaus effect in bulk wurtzite materials. *Appl. Phys. Lett.* **91,** 082110 (2007).
23. Cartoixà, X., Ting, D. Z-Y. & Chang, Y-C. Suppression of the D'yakonov-Perel' spin-relaxation mechanism for all spin components in [111] zincblende quantum wells. *Phys. Rev. B* **71,** 045313 (2005).
24. Seah, M. P. & Dench, W. A. Quantitative electron spectroscopy of surfaces: A standard data base for electron inelastic mean free paths in solids. *Surf. Interface Anal.* **1,** 2–11 (1979).

25. Takeda, S. N., Higashi, N. & Daimon, H. Visualization of in-plane dispersion of hole subbands by photoelectron spectroscopy. *Phys. Rev. Lett.* **94,** 037401 (2005).
26. King, P. D. C. *et al.* Surface band-gap narrowing in quantized electron accumulation layers. *Phys. Rev. Lett.* **104,** 256803 (2010).
27. King, P. D. C., Veal, T. D. & McConville, C. F. Nonparabolic coupled Poisson–Schrödinger solutions for quantized electron accumulation layers: Band bending, charge profile, and subbands in InN surfaces. *Phys Rev. B* **77,** 125305 (2008).
28. Edelstein, V. M. Spin polarization of conduction electrons induced by electric current in two-dimensional asymmetric electron systems. *Solid State Commun.* **73,** 233–235 (1990).
29. Miron, I. M. *et al.* Current-driven spin torque induced by the Rashba effect in a ferromagnetic metal layer. *Nature Mater.* **9,** 230–234 (2010).
30. Kiss, T. *et al.* A versatile system for ultrahigh resolution, low temperature, and polarization dependent laser-angle-resolved photoemission spectroscopy. *Rev. Sci. Instrum.* **79,** 023106 (2008).
31. Iori, K. *et al.* The self-calibration of a retarding-type Mott spin polarimeter with a large collection angle. *Rev. Sci. Instrum.* **77,** 013101 (2006).
32. Blaha, P., Shwarz, K., Madsen, G., Kvasnicka, D. & Luiz, J. WIEN2K package; available at, http://www.wien2k.at.
33. Perdew, J. P., Burke, K. & Ernzerhof, M. Generalized gradient approximation made simple. *Phys. Rev. Lett.* **77,** 3865–3868 (1996).
34. Mostofi, A. A., Yates, J. R., Lee, Y-S., Vanderbilt, D. & Marzari, N. Wannier90: A tool for obtaining maximally localized Wannier functions. *Comp. Phys. Commun.* **178,** 685–699 (2008).
35. Kuneš, J. *et al.* WIEN2WANNIER: From linearized augmented plane waves to maximally localized Wannier functions. *Comp. Phys. Commun.* **181,** 1888–1895 (2010).
36. Dil, J. H. *et al.* Rashba-type spin–orbit splitting of quantum well states in ultrathin Pb films. *Phys. Rev. Lett.* **101,** 266802 (2008).
37. Hirahara, T. *et al.* Quantum well states in ultrathin Bi films: Angle-resolved photoemission spectroscopy and first-principles calculations study. *Phys. Rev. B* **75,** 035422 (2007).

Acknowledgements

We thank H. Y. Hwang and J. S. Lee for discussion, and Y. Ishida for his help in the ARPES experiment. This research is supported by the Japan Society for the Promotion of Science through the 'Funding Program for World-Leading Innovative R&D on Science and Technology (FIRST Program)', initiated by the Council for Science and Technology Policy.

Author contributions

K.I., M.S., T. Shimojima and T. Sonobe carried out (SR)ARPES. K. Koizumi and S.S. shared the ARPES infrastructure at the Institute of Solid State Physics and assisted with measurements. H.M., A.K., K.M., T.O., H.N. and M.T. shared the SRARPES infrastructure at the Hiroshima Synchrotron Radiation Center and assisted with measurements. M.S.B., R.A. and N.N. carried out the calculations. K. Kobayashi, Y.M. and R.K. carried out X-ray diffraction and determined the crystal structure. H.M., Y.K. and Y.O. carried out the crystal growth and transport measurements. K.I. analysed the (SR)ARPES data and wrote the manuscript with input from M.S.B., H.M., R.A., N.N. and Y.T. Y.T. conceived and coordinated the project.

Additional information

The authors declare no competing financial interests. Reprints and permissions information is available online at http://www.nature.com/reprints. Correspondence and requests for materials should be addressed to K.I.